

## RESEARCH ARTICLE

# Synthesis and Preliminary Evaluation of Piperidinyl and Pyrrolidinyl Iodobenzoates as Imaging Agents for Butyrylcholinesterase

Ian R. Macdonald,<sup>1</sup> G. Andrew Reid,<sup>1</sup> E. Eric Joy,<sup>2</sup> Ian R. Pottie,<sup>2,3</sup> Gilbert Matte,<sup>4</sup> Steven Burrell,<sup>4</sup> George Mawko,<sup>4</sup> Earl Martin,<sup>2</sup> Sultan Darvesh<sup>1,2,5</sup>

<sup>1</sup>Department of Anatomy and Neurobiology and the Neuroscience Institute, Dalhousie University, Halifax, NS, B3H 1X5, Canada

<sup>2</sup>Department of Chemistry and Physics, Mount Saint Vincent University, Halifax, Nova Scotia, B3M 2J6, Canada

<sup>3</sup>Department of Chemistry, Saint Mary's University, Halifax, Nova Scotia, B3H 3C3, Canada

<sup>4</sup>Department of Radiology, Dalhousie University, Halifax, Nova Scotia, B3H 1X5, Canada

<sup>5</sup>Department of Medicine (Neurology and Geriatric Medicine), Dalhousie University, Halifax, Nova Scotia, B3H 1X5, Canada

### Abstract

**Purpose:** The purpose of this study is to synthesize and evaluate specific agents for molecular imaging of butyrylcholinesterase (BuChE), known to be associated with neuritic plaques and neurofibrillary tangles in Alzheimer's disease (AD). In this study, these agents were tested in a normal rat model. The distribution of radiolabel was compared with known BuChE histochemical distribution in the rat brain.

**Procedures:** Iodobenzoate esters were synthesized and tested, through spectrophotometric analysis, as specific substrates for BuChE. These compounds were converted to the corresponding <sup>123</sup>I esters from tributyltin intermediates and purified for studies in the rat model. Whole body dynamic scintigraphic images were obtained for biodistribution studies. Autoradiograms of brain sections were obtained and compared to histochemical distribution of the enzyme in this model system.

**Results:** The three iodobenzoate esters studied were specific substrates for BuChE. Whole body biodistribution studies with <sup>123</sup>I-labeled compounds showed rapid disappearance from the body while radioactivity was retained in the head region. Brain section autoradiography of animals injected with these labeled compounds indicated that most areas known to contain BuChE corresponded to areas of radioactivity accumulation.

**Conclusion:** BuChE-specific radiolabeled iodobenzoates enter the brain and, in general, label areas known to exhibit BuChE activity in histochemical studies. Such molecules may represent a new direction for the development of agents for the molecular imaging of BuChE in the living brain, especially in regions where BuChE-containing neuropathological structures appear in AD.

**Key words:** Butyrylcholinesterase, Alzheimer's disease, Brain SPECT, Tributyltin, <sup>123</sup>Iodine, Amyloid plaques, Neurofibrillary tangles

### Introduction

Currently, a definitive diagnosis of Alzheimer's disease (AD) requires the detection of dementia and demonstration of characteristic AD pathology, amyloid plaques, and neurofibrillary tangles, at autopsy [1, 2]. Accurate

diagnosis of AD in patients during life is imperative to initiate early treatment and to monitor treatment effects.

In AD brains, there is widespread cell loss and, in particular, loss of cholinergic neurons [3], leading to a decrease in the enzyme choline acetyltransferase and its product, the neurotransmitter, acetylcholine. This loss is responsible, in part, for the characteristic cholinergic dysfunction in AD [4, 5]. An enzyme regulating acetylcholine, acetylcholinesterase (AChE, EC 3.1.1.7), also shows significant loss in AD brains [6]. However, activity of the related enzyme, butyrylcholinesterase (BuChE, EC 3.1.1.8), also able to catalyze acetylcholine hydrolysis, has been observed to increase in AD [6].

In the healthy brain, AChE is found in neurons and neuropil [7] while BuChE is found in white matter, glia, and specific populations of neurons [8–11]. In AD brain tissue, AChE and BuChE are also associated with amyloid plaques, predominantly located in the cerebral cortex [12–17]. This association should allow molecular imaging of AD pathology during life using cholinesterase-specific radiolabeled compounds. However, in normal and AD cerebral cortex, the distribution of BuChE (Fig. 1a, d), AChE (Fig. 1b, e), and  $\beta$ -amyloid (Fig. 1c, f) indicates that compounds specific for BuChE, rather than AChE, would be more suitable for imaging AD pathology. BuChE and  $\beta$ -amyloid levels are both low in normal cerebral cortex (Fig. 1a, c) and high in AD cerebral cortex (Fig. 1d, f). However, AChE levels are comparably high in both normal (Fig. 1b) and AD (Fig. 1e) cerebral cortex and would make it difficult to distinguish normal from AD with AChE neuroimaging. BuChE activity associated with AD pathology, in areas of the brain where this enzyme is not normally prominent, suggests that visualizing BuChE activity by neuroimaging could be valuable in detection of AD pathology in the living brain. This could facilitate early diagnosis of AD during life.

Synthesis and evaluation of BuChE-specific radiolabeled imaging agents, derived from *N*-methylpyrrolidinol and *N*-methylpiperidinol have been previously reported [18–20]. One such molecule, predicted to be BuChE-specific, 1- $^{11}\text{C}$ -methyl-4-piperidinyl *n*-butyrate ( $^{11}\text{C}$ -MP4B), was developed for PET imaging. Biodistribution studies with  $^{11}\text{C}$ -MP4B, performed in the human brain [21] and other organs [22], indicated high initial brain uptake but with a rapid clearance over 30 min [21]. Most significant, labeling did not correlate [23] with the known histochemical localization of BuChE in normal [8–11] or in AD brains [12–17]. A possible reason for this lack of correlation is that in  $^{11}\text{C}$ -MP4B, the radioisotope is located on the part of the substrate that is the initial leaving group in the mechanism of BuChE catalysis.

In an effort to prevent early loss of radiolabel from the BuChE–substrate complex, we incorporated a radioactive marker on the acyl moiety of the ester, the last component of the substrate to dissociate from the enzyme following hydrolysis. To develop BuChE-specific imaging agents that would have the potential to remain bound longer, 4-iodobenzoate derivatives of *N*-methylpyrrolidinol and *N*-

methylpiperidinol were prepared and evaluated. The rationale for synthesizing these compounds was that the size of the iodobenzoate moiety should render such esters more susceptible to hydrolysis by BuChE over AChE. Also, the iodo group on the acyl portion of the molecule should be amendable to subsequent exchange with  $^{123}\text{I}$ . Lastly, previous studies have shown that chemical structures that contain *N*-methylpyrrolidinol or *N*-methylpiperidinol moiety readily enter the brain [20, 21, 23]. To evaluate whether these radiolabeled compounds could be used for imaging BuChE activity in the brain, a normal rat model system was employed in the present study to examine whole body biodistribution while brain autoradiograms were used to compare radiolabel distribution to the known histochemical distribution of BuChE in the rat brain [24, 25].

---

## Material and Methods

### Materials

Butyl lithium, 1-methylpiperidin-4-ol, (*S*)-1-methylpyrrolidin-3-ol, (*R*)-1-methylpyrrolidin-3-ol, 4-iodobenzoyl chloride, hexabutyliditin, tetrakis(triphenylphosphine)palladium, and purified recombinant human acetylcholinesterase were obtained from Sigma-Aldrich. Purified human plasma butyrylcholinesterase was a gift from Dr. Oksana Lockridge.  $\text{Na}^{123}\text{I}$  was obtained from MDS Nordion in 0.1 N NaOH. Synthetic reactions were performed under an argon atmosphere (99.999% purity, Air Liquide). Male wistar rats were purchased from Charles River Laboratories (Canada) and aged until 3–6 months old.

### Chemical Analysis of Synthetic Compounds

Melting points were determined using a Fisher-Johns Melting Point Apparatus. Infrared spectra were recorded as Nujol mulls or as neat liquids between sodium chloride plates on a Nicolet Avatar 330 FT-IR spectrometer. Peak positions were reproducible within 1–2  $\text{cm}^{-1}$ . Nuclear magnetic resonance spectra were recorded at the Nuclear Magnetic Resonance Research Resource (NMR-3), Dalhousie University, on a Bruker AVANCE 500, operating at 500.1 MHz for  $^1\text{H}$  and 125.8 MHz for  $^{13}\text{C}$ . Chemical shifts are reported in parts per million relative to  $\text{Me}_4\text{Si}$  in  $\text{CDCl}_3$  or DMSO. For Proton NMR experiments, the coupling constants are reported in Hertz and the multiplicities are apparent. For Carbon NMR data, the number of attached protons for each signal, as determined by a DEPT experiment, are given in parentheses. Low-resolution mass spectra were obtained using an Agilent 6890N GC with an Agilent 6890N Electron Impact MS (Waldbronn, Germany) operating at 70 eV. High-resolution mass spectra were obtained with accurate mass positive-ion electrospray ionization measurements recorded at the Mass Spectrometry Laboratory at Dalhousie University using a Bruker Daltonics microTOF with a flow rate of 2  $\mu\text{L}/\text{min}$ , spray voltage of 4,500 V and tray temperature of 180°C or were recorded on a CEC 21-110B spectrometer using electron ionization at 70 V and an appropriate source temperature with samples being introduced by means of a heatable port probe. Mass measurements

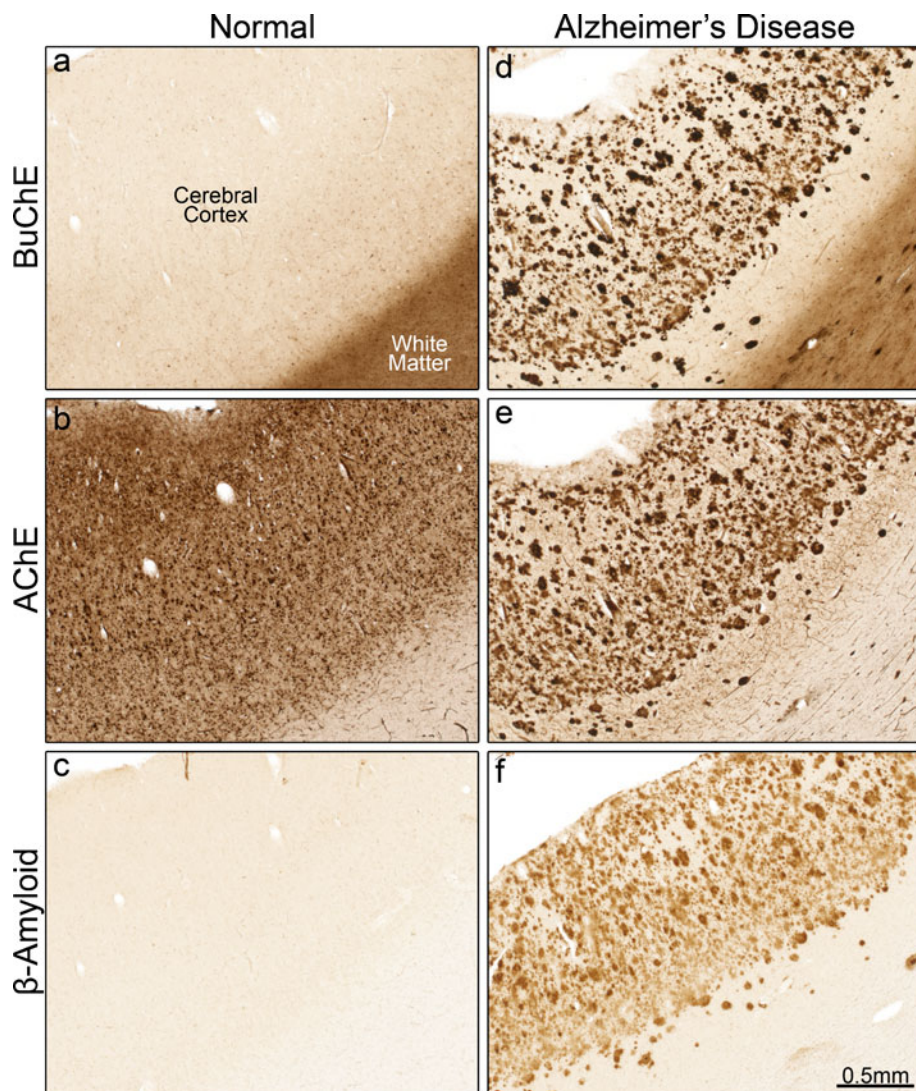


**Fig. 1.** Photomicrographs of butyrylcholinesterase (*BuChE*), acetylcholinesterase (*AChE*), and  $\beta$ -amyloid staining in normal (**a–c**) and Alzheimer's disease (**d–f**) cerebral cortex. Note similar plaque staining with *BuChE* (**d**), *AChE* (**e**), and  $\beta$ -amyloid (**f**) in AD. These structures are absent in normal brain (**a–c**). In normal brain there is a low level of *BuChE* (**a**) in the cortex and no  $\beta$ -amyloid plaques (**c**) while there is relatively intense *AChE* staining (**b**). These differences make *BuChE* a suitable target over *AChE* for imaging AD pathology. *BuChE* and *AChE* histochemistry was done as described previously [17].  $\beta$ -amyloid was stained using a standard immunohistochemical technique.

were within 3 ppm of the calculated value. Purity of all compounds was determined using an Agilent Technologies 1200 series HPLC system with a reverse phase C18 column and methanol as the mobile phase.

### Synthesis of Non-radioactive Piperidinol and Pyrrolidinol Iodobenzoate Derivatives

The non-radioactive 4-iodobenzoate esters of *N*-methylpiperidinol (**1**) and (*S*) and (*R*) *N*-methylpyrrolidinol (**2** and **3**, respectively) were synthesized according to the reaction scheme depicted in Fig. 2a.

For synthesis of 1-methylpiperidin-4-yl 4-iodobenzoate (**1**), under an argon atmosphere, 1-methylpiperidin-4-ol (0.3837 g, 3.331 mmol) was dissolved in tetrahydrofuran (THF; 20 mL). To

this solution was added butyl lithium (BuLi; 2.10 mL, 3.36 mmol) at  $-78^{\circ}\text{C}$  followed by a solution of 4-iodobenzoyl chloride (0.8002 g, 3.003 mmol) in THF (10 mL) and the mixture was stirred at room temperature for 16 h. The reaction was quenched with water (20 mL) and extracted with ethyl acetate ( $3 \times 20$  mL). The combined organic layers were washed with brine ( $2 \times 20$  mL) and dried over  $\text{Na}_2\text{SO}_4$ . The solvent was removed *in vacuo* to produce a white solid. The product was purified by silica gel chromatography (30:70 MeOH/ $\text{CH}_2\text{Cl}_2$ ) to give a white powder (0.5561 g, 54%). Analytical data: MP:  $128\text{--}130^{\circ}\text{C}$  (Lit MP= $130^{\circ}\text{C}$  [26]). IR (Nujol): 1711, 1585, 1283, 1268, 1118, and  $754\text{ cm}^{-1}$ .  $^1\text{H-NMR}$  ( $\text{CDCl}_3$ ):  $\delta$  1.84–1.91 (m, 2H), 2.01–2.08 (m, 2H), 2.31–2.39 (m, 5H), 2.67–2.73 (m, 2H), 5.02–5.08 (m, 1H), 7.75 (d,  $J=8.5$  Hz, 2H), and 7.81 (d,  $J=8.5$  Hz, 2H).  $^{13}\text{C-NMR}$  ( $\text{CDCl}_3$ ):  $\delta$  31, 46, 53, 70, 100, 130, 131, 138, and 166. EI-MS  $m/z$ : 55, 70, 82, 97, 114, 203, 231, and 345 ( $\text{M}^+$ ). HRMS (ESI):  $\text{M}^+$  found 345.0233, calcd for  $\text{C}_{13}\text{H}_{16}\text{NO}_2\text{I}$ =345.0226.

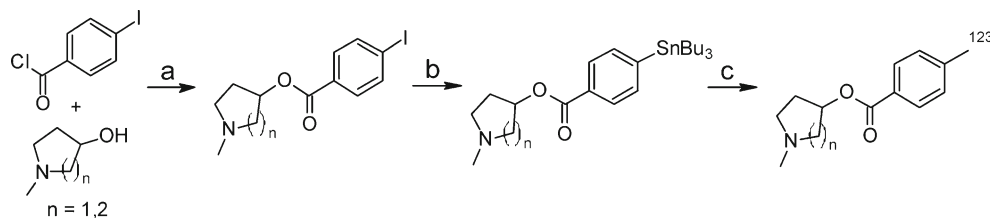


**Fig. 2.** Synthetic reaction scheme for the non-radioactive esters, tributyltin intermediates and  $^{123}\text{I}$ -labeled esters, respectively. For the *N*-methylpyrrolidinols ( $n=1$ ), compounds were enantiomerically pure. (a) BuLi and THF. (b)  $\text{Sn}_2\text{Bu}_6$ ,  $\text{Pd}(\text{PPh}_3)_4$ , and THF. (c)  $\text{Na}^{123}\text{I}$ , NCS, and MeOH.

For synthesis of (*S*)-1-methylpyrrolidin-3-yl 4-iodobenzoate (**2**), under an argon atmosphere, (*S*)-1-methylpyrrolidin-3-ol (0.257 mL, 2.52 mmol) was dissolved in THF (10 mL). To this solution was added BuLi (1.60 mL, 2.56 mmol) at  $-78^\circ\text{C}$  followed by a solution of 4-iodobenzoyl chloride (0.5870 g, 2.203 mmol) in THF (10 mL). The solution was refluxed for 3 h and the reaction was quenched with water (15 mL). The aqueous layer was extracted with ethyl acetate ( $2 \times 10$  mL), washed with brine ( $2 \times 15$  mL) and dried over  $\text{MgSO}_4$ . The solvent was removed *in vacuo* and the product was recrystallized from hexanes to yield yellow crystals (0.3053 g, 41%). Analytical data: MP<sub>(hexanes)</sub>:  $69\text{--}70^\circ\text{C}$ . IR (Nujol) 1723, 1586, 1268, 1235, 1115, and  $754\text{ cm}^{-1}$ .  $^1\text{H-NMR}$  ( $\text{CDCl}_3$ ):  $\delta$  1.99–2.03 (m, 1H), 2.37–2.42 (m, 5H), 2.77–2.81 (m, 1), 2.83 (d,  $J=2.6$  Hz, 1H), 2.85–2.88 (m, 1H), 5.40–5.43 (m, 1H), 7.75 (dt,  $J=2.0, 8.7$  Hz, 2H), and 7.79 (dt,  $J=2.0, 8.7, 2\text{H}$ ).  $^{13}\text{C-NMR}$  ( $\text{CDCl}_3$ ):  $\delta$  33 (3), 42 (1), 55 (1), 62 (2), 76 (2), 101 (0), 130 (0), 131 (1), 138 (1), and 166 (0). EI-MS  $m/z$ : 42, 58, 74, 83, 104, 203, and 231 ( $\text{M}^+-101$ ,  $\text{C}_7\text{H}_4\text{IO}$ ). HRMS (ESI):  $\text{M}^+\text{H}^+$  found 332.0142; calcd for  $\text{C}_{12}\text{H}_{14}\text{NO}_2\text{I}=332.0147$ .

For synthesis of (*R*)-1-methylpyrrolidin-3-yl 4-iodobenzoate (**3**), under an argon atmosphere, (*R*)-1-methylpyrrolidin-3-ol (0.260 mL, 2.37 mmol) was dissolved in THF (10 mL). To this solution was added BuLi (1.60 mL, 2.56 mmol) at  $-78^\circ\text{C}$  followed by a solution of 4-iodobenzoyl chloride (0.5932 g, 2.226 mmol) in THF (10 mL). The solution was refluxed for 3 h and the reaction was quenched with water (15 mL). The aqueous layer was extracted with ethyl acetate ( $2 \times 10$  mL), washed with brine ( $2 \times 15$  mL), and dried over  $\text{MgSO}_4$ . The solvent was removed *in vacuo* and the product was recrystallized from hexanes to yield light yellow crystals (0.3696 g, 51%). Analytical data: MP<sub>(hexanes)</sub>:  $69\text{--}70^\circ\text{C}$ . IR (Nujol): 1724, 1586, 1268, 1235, 1115, and  $754\text{ cm}^{-1}$ .  $^1\text{H-NMR}$  ( $\text{CDCl}_3$ ):  $\delta$  2.00–2.03 (m, 1H), 2.37–2.42 (m, 5H), 2.77–2.81 (m, 1H), 2.83 (d,  $J=2.6$  Hz, 1H), 2.84–2.88 (m, 1H), 5.31–5.43 (m, 1H), 7.76 (dt,  $J=1.9, 8.5$  Hz, 2H), and 7.80 (dt,  $J=1.7, 8.6$  Hz, 2H).  $^{13}\text{C-NMR}$  ( $\text{CDCl}_3$ ):  $\delta$  33 (2), 42 (3), 55 (2), 62 (2), 76 (1), 101 (0), 130 (0), 131 (1), 138 (1), and 166 (0). EI-MS  $m/z$ : 42, 58, 74, 83, 104, 203, and 231 ( $\text{M}^+-101$ ,  $\text{C}_7\text{H}_4\text{IO}$ ). HRMS (ESI):  $\text{M}^+\text{H}^+$  found 332.0142; calcd for  $\text{C}_{12}\text{H}_{14}\text{NO}_2\text{I}=332.0147$ .

### Synthesis of Tributyltin Intermediates

The synthesis of tributyltin intermediates was carried out as depicted in Fig. 2b.

For synthesis of 1-methylpiperidin-4-yl 4-(tributylstannyl)benzoate intermediate, under argon atmosphere, 1-methylpiperidin-4-yl 4-iodobenzoate (**1**) (0.1660 g, 0.4810 mmol) was dissolved in degassed toluene (40 mL). Hexabutyliditin (0.60 mL, 1.198 mmol) was added, followed by a solution containing tetrakis(triphenyl-

phosphine)palladium (0.0303 g, 0.0262 mmol), also dissolved in degassed toluene (15 mL). The resulting solution was refluxed for 20 h and the solvent removed *in vacuo*. The product was purified by silica gel column chromatography (15:1 toluene/triethylamine) to yield a viscous yellow liquid (0.1795 g, 71%). Analytical data: IR (Neat): 1717, 1590, 1275, 1104, and  $752\text{ cm}^{-1}$ .  $^1\text{H-NMR}$  ( $\text{CDCl}_3$ ):  $\delta$  0.88 (t,  $J=7.3$  Hz, 9H), 1.08 (p,  $J=6.3$  Hz, 6H), 1.36 (sext,  $J=7.4$  Hz, 6H), 1.57 (p,  $J=7.6$  Hz, 6H), 1.89–1.94 (m, 2H), 2.03–2.08 (m, 2H), 2.36 (s, 3H), 2.37–2.39 (m, 2H), 2.69–2.72 (m, 2H), 5.09–5.10 (m, 1H), 7.59 (d,  $J=8.1$  Hz, 2H), and 8.00 (d,  $J=8.1$  Hz, 2H).  $^{13}\text{C-NMR}$  ( $\text{CDCl}_3$ ):  $\delta$  10 (2), 13 (3), 27 (2), 29 (2), 31 (2), 46 (3), 53 (2), 70 (1), 128 (1), 130 (0), 136 (1), 149 (0), and 166 (0). EI-MS  $m/z$ : 41, 55, 82, 96, 170, 198, 241, 340, 396, and 452 ( $\text{M}^+-57$ ,  $\text{C}_{21}\text{H}_{34}\text{NO}_2\text{Sn}$ ). HRMS (ESI):  $\text{M}^+\text{H}^+$  found 510.2389; calcd for  $\text{C}_{25}\text{H}_{44}\text{NO}_2\text{Sn}=510.2394$ .

For synthesis of (*S*)-1-methylpyrrolidin-3-yl 4-(tributylstannyl)benzoate intermediate, under argon atmosphere, (*S*)-1-methylpyrrolidin-3-yl 4-iodobenzoate (**2**) (0.1001 g, 0.3022 mmol) was dissolved in degassed toluene (30 mL) and hexabutyliditin (0.355 mL, 0.709 mmol) was added. Tetrakis(triphenylphosphine)palladium (0.0107 g, 0.0092 mmol) also dissolved in toluene (15 mL) was added. The resulting solution was refluxed for 20 h and the solvent removed *in vacuo*. The resulting crude product was purified by silica gel column chromatography (11:8:1, hexanes/ethyl acetate/triethylamine) to yield a viscous yellow liquid (0.1157 g, 78%). Analytical data: IR (Neat): 1717, 1591, 1275, 1105, and  $752\text{ cm}^{-1}$ .  $^1\text{H-NMR}$  (DMSO):  $\delta$  0.85 (t,  $J=7.5$  Hz, 9H), 1.08 (p,  $J=7.6, 8.2$  Hz, 6H), 1.28 (sext,  $J=7.4$  Hz, 6H), 1.51 (p,  $J=7.3$  Hz, 6H), 1.83–1.86 (m, 1H), 2.26 (s, 3H), 2.28–2.31 (m, 2H), 2.63–2.66 (m, 1H), 2.69–2.72 (m, 2H), 5.25–5.27 (m, 1H), 7.56 (d,  $J=7.9$  Hz, 2H), and 7.82 (d,  $J=7.9$  Hz, 2H).  $^{13}\text{C-NMR}$  (DMSO):  $\delta$  9 (2), 13 (3), 27 (2), 28 (2), 32 (2), 42 (3), 54 (2), 62 (2), 75 (1), 128 (1), 129 (0), 136 (1), 149 (0), and 166 (0). EI-MS  $m/z$ : 42, 58, 83, 105, 196, 241, 326, 382, and 438 ( $\text{M}^+-57$ ,  $\text{C}_{20}\text{H}_{32}\text{NO}_2\text{Sn}$ ). HRMS (ESI):  $\text{M}^+\text{H}^+$  found 496.2232; calcd for  $\text{C}_{24}\text{H}_{42}\text{NO}_2\text{Sn}=496.2238$ .

For synthesis of (*R*)-1-methylpyrrolidin-3-yl 4-(tributylstannyl)benzoate intermediate, under argon atmosphere, (*R*)-1-methylpyrrolidin-3-yl 4-iodobenzoate (**3**) (0.1010 g, 0.3050 mmol) was dissolved in degassed toluene (30 mL) and hexabutyliditin (0.355 mL, 0.709 mmol) was added. Tetrakis(triphenylphosphine)palladium (0.0105 g, 0.0091 mmol) dissolved in toluene (15 mL) was added. The resulting solution was refluxed for 20 h and the solvent removed *in vacuo*. The resulting crude product was purified by silica gel column chromatography (11:8:1, hexanes/ethyl acetate/triethylamine) to yield a viscous yellow liquid (0.1150 g, 78%). Analytical data: IR (Neat): 1717, 1591, 1275, 1104, and  $752\text{ cm}^{-1}$ .  $^1\text{H-NMR}$  ( $\text{CDCl}_3$ ):  $\delta$  0.94 (t,  $J=7.4$  Hz, 9H), 1.13 (p,  $J=7.9, 8.2$  Hz, 6H), 1.37 (sext,  $J=7.3$  Hz, 6H), 1.57 (p,  $J=7.9, 8.2$  Hz, 6H), 2.08–2.13 (m, 1H), 2.43–2.47 (m, 2H), 2.52 (s, 3H), 2.90–2.93 (m, 2H), 5.45–5.48 (m, 1H), 7.54 (d,  $J=8$  Hz, 2H), and

7.96 (d,  $J=8$  Hz, 2H).  $^{13}\text{C}$ -NMR ( $\text{CDCl}_3$ ):  $\delta$  10 (2), 14 (3), 28 (2), 29 (2), 31 (2), 43 (3), 56 (2), 63 (2), 75 (1), 129 (1), 133 (0), 137 (1), 150 (0), and 167 (0). EI-MS  $m/z$ : 42, 58, 83, 105, 196, 241, 326, 382, and 438 ( $\text{M}^+-57$ ,  $\text{C}_{24}\text{H}_{42}\text{NO}_2\text{Sn}$ ). HRMS (ESI):  $\text{M}^+\text{H}^+$  found 496.2232; calcd for  $\text{C}_{24}\text{H}_{42}\text{NO}_2\text{Sn}$ =496.2238.

### *In Vitro Evaluation of Non-radioactive Iodobenzoates as Cholinesterase Ligands*

The specificity, affinity, and rate of hydrolysis of each synthetic compound were determined spectrophotometrically, making use of differences in the aryl chromophores of substrates and products. Briefly, 15  $\mu\text{L}$  of AChE (9 U) or BuChE (9 U) dissolved in 0.1% gelatin<sub>(aq)</sub>, containing 0.01% sodium azide, and 1.44 mL of 0.1 M phosphate buffer (pH 8.0) were placed in a quartz cuvette of 1 cm path length. The reaction was commenced with the addition of 50  $\mu\text{L}$  of 5 mM substrate (**1**, **2**, or **3**) in 50% acetonitrile<sub>(aq)</sub>. The absorbance was scanned from 200–300 nm every 2 min for a total of 30 min using a Ultrospec 2100 pro UV/Visible Spectrophotometer (Biochrom) with Swift II software (Amersham). The wavelength corresponding to the maximum absorbance change for each compound during hydrolysis was used for the subsequent determination of affinity constant ( $K_m$ ) and maximum velocity ( $V_{\text{max}}$ ), using Lineweaver-Burk double reciprocal plots. This was accomplished by measuring the change in absorbance per min ( $\Delta A/\text{min}$ ), using a fixed amount of enzyme (2.7 U) and varying amounts of compounds **1–3** ( $1.67 \times 10^{-5}$ – $1.67 \times 10^{-4}$  M), using a Spectronic 1001 (Milton Roy). The plot of  $1/v$  against  $1/s$  gave  $K_m$  as the negative reciprocal of the intercept on the  $1/s$ -axis and  $V_{\text{max}}$  as the reciprocal of the  $1/v$ -axis intercept. As defined previously, 0.1 U is the amount of cholinesterase that gives a  $\Delta A/\text{min}$  of 1.0 in the presence of  $1.6 \times 10^{-4}$  M substrate (acetylthiocholine for AChE, butyrylthiocholine for BuChE) [27].

### *Computation of Preferred Conformations and Log P Values*

Computational chemistry studies, to determine the most stable geometries of compounds **1–3**, were carried out at the molecular mechanics level of theory using the Merck Molecular Force Field, employing Spartan '06 [28].

Log P values were calculated to assess the ability of the compound to cross the blood–brain barrier by diffusion. The values were obtained using ALOGPS v 2.0 system method that compares the structure of the molecule with a large database of known molecular partition coefficients [29].

### *Radiosynthesis and Purification of $^{123}\text{I}$ -Labeled Iodobenzoates*

Substrates labeled with  $^{123}\text{I}$  were prepared from tributyltin intermediates according to the general scheme shown in Fig. 2c. To a solution (8  $\mu\text{L}$ ) of  $\text{Na}^{123}\text{I}$  (68.45 MBq) in 0.1 M  $\text{NaOH}_{(\text{aq})}$  ( $8.0 \times 10^{-4}$  mol) was added  $\text{NaI}$  (3  $\mu\text{L}$ ,  $5.5 \times 10^{-9}$  mol) and 0.1 M  $\text{HCl}$  (16  $\mu\text{L}$ ,  $1.6 \times 10^{-3}$  mol) to neutralize the hydroxide. The tributyltin intermediate (50  $\mu\text{L}$ ,  $4.0 \times 10^{-7}$  mol) was added to this solution, followed by *N*-chlorosuccinimide (28  $\mu\text{L}$ ,  $8.4 \times 10^{-8}$  mol),

both of which were dissolved in methanol. The reaction proceeded for 15 min at room temperature; then 0.1 M  $\text{NaHCO}_3$  (24  $\mu\text{L}$ ,  $2.4 \times 10^{-3}$  mol) was added to quench the reaction. Purification was accomplished by HPLC, using a Waters system with a ZORBAX Eclipse XDB-C18,  $4.6 \times 250$  mm, 5  $\mu\text{m}$  column (Agilent Technologies), and 1.0 mL/min of 80% methanol<sub>(aq)</sub> eluent. Fractions were collected every 20 s for 20 min with a RediFrac fraction collector (Amersham Biosciences). Retention times were determined using the corresponding cold iodobenzoate as a non-radioactive standard. Collected fractions that contained purified product were combined and the solvent removed under a stream of  $\text{N}_2$  gas. The product was redissolved either with methanol, to assess the radiochemical yield and purity, or in 20% ethanol<sub>(aq)</sub>, for animal administration.

### *Animal Studies*

Animals were cared for according to the guidelines set by the Canadian Council on Animal Care. Formal approval to conduct the experiments was obtained from the Dalhousie University Committee on Laboratory Animals.

### *Biodistribution Studies of Radiolabeled Iodobenzoates*

Whole body dynamic scintigraphic imaging of male wistar rats (~500 g) were obtained. The animals were anesthetized using a constant stream of isoflurane gas and the tail vein was cannulated. The animals were positioned on the head of a gamma camera (Millennium MG; GE Healthcare) equipped with a low-energy high-resolution parallel-hole collimator. Immediately following injection of the radiolabeled compound (~37 MBq), counts were acquired by the gamma camera in dynamic frame mode (energy window centered on the 159 keV photopeak of  $^{123}\text{I}$ ;  $128 \times 128$  pixels frame matrix;  $180 \times 5$  s, and  $45 \times 60$  s frames, for a total of 60 min). At the end of the 1 h imaging period, the animals were sacrificed with sodium pentobarbital. Regions of interest (ROI) representing the head (ROI<sub>1</sub>), heart (ROI<sub>2</sub>), and bladder (ROI<sub>3</sub>) were manually defined on the whole body image using the gamma camera's workstation image edit tools (Xeleris version 2.1220; GE Healthcare). Background- and radioactive decay-corrected ROI time activity curves were calculated and plotted, using the same tools, showing the percentage fraction of the injected dose as a function of time in the organ. The whole body counting rate from minute 1 to minute 5 was used to estimate the total injected activity.

### *Brain Autoradiography*

Animals were prepared as described for the biodistribution studies, except that the body temperature was maintained on a circulating water heating pad set at 40°C for the duration of the experiment. The radiolabeled ligand was administered (~37 MBq) and after 30 min the animals were sacrificed by an injection of sodium pentobarbital (0.3 mL). The animals were immediately perfused transcardially with 200 mL of isotonic saline followed by 500 mL of 4% paraformaldehyde in 0.1 M phosphate buffer, pH 7.4. The brains were quickly removed and immediately frozen using dry ice. The brains were sectioned in 100- $\mu\text{m}$  thick coronal slices on a

SM2000R Leica microtome with a freezing stage and BFS-30TC controller (Physitemp) and immediately mounted on glass slides. The slides were then placed under a phosphor imaging screen (Molecular Dynamics). After 36 h, the screen was visualized using a Typhoon 9410 Phosphorimager (GE Healthcare) to produce the autoradiogram. A color gradient was placed on autoradiograms in Adobe Photoshop 7 to highlight areas with radioactivity. Three animals underwent this procedure for each of the three radiolabeled compounds.

### Butyrylcholinesterase Histochemistry

A modified Karnovsky-Roots method was used for examination of butyrylcholinesterase activity in brain sections, as described previously [17]. Briefly, 40- $\mu\text{m}$  brain sections were rinsed in 0.1 M maleate buffer (pH 7.4) for 30 min and reacted for 3 h at 37°C in an incubation medium containing 0.5 mM sodium citrate, 0.47 mM cupric sulfate, 0.05 mM potassium ferricyanide, 0.8 mM butyrylthiocholine iodide, and 0.01 mM 1,5-bis (4-allyl dimethylammonium phenyl) pentan-3-one dibromide (BW 284 C 51) in 0.1 M maleate buffer (pH 8.0) for BuChE staining. Sections were rinsed with gentle agitation for 30 min in distilled water and placed in 0.1% cobalt(II) chloride in water for 10 min. After a further rinsing in distilled water, sections were placed in a solution of 1.39 mM 3,3'-diaminobenzidine tetrahydrochloride (DAB) in 0.1 M phosphate buffer (pH 7.4). After 5 min, a solution of 0.3% hydrogen peroxide in distilled water was added at a ratio of 20:1 (DAB solution : hydrogen peroxide solution) and the reaction was carried out for approximately 4 min. Sections were then washed in 0.1 M acetate buffer (pH 3.3) mounted on slides, coverslipped, and examined with brightfield microscopy.

Sections were photographed on a Zeiss Axioplan 2 motorized microscope with a Zeiss Axiocam HRC digital camera and AxioVision 4.6 software. Image levels were adjusted in Adobe Photoshop 7 so the background from different images matched.

## Results

Three non-radiolabeled iodobenzoate esters were synthesized and tested *in vitro* for their ability to bind to, and be hydrolyzed by, BuChE and AChE. Lack of AChE hydrolysis for each compound confirmed specificity for BuChE. All three BuChE-specific substrates studied were then radiolabeled and evaluated *in vivo* and *ex vivo* using whole body dynamic scintigraphic imaging and brain autoradiography, respectively.

### Synthesis of Non-radioactive Iodobenzoate Derivatives

1-methylpiperidin-4-yl 4-iodobenzoate (**1**), (*S*)-1-methylpyrrolidin-3-yl 4-iodobenzoate (**2**), and (*R*)-1-methylpyrrolidin-3-yl 4-iodobenzoate (**3**) (Table 1), were synthesized (Fig. 2a) in moderate (41–54%) yields and were found to be  $\geq 97\%$  pure by HPLC analysis. Chemical analysis of each was consistent with its structure. All three derivatives synthesized had similar calculated log P values (Table 1), com-

parable to compounds known to cross blood–brain barrier [30].

### *In Vitro* Evaluation of Non-radioactive Iodobenzoates as Cholinesterase Ligands

The three purified and characterized compounds (**1–3**) were evaluated *in vitro* as substrates for human AChE and BuChE, making use of the natural chromophores of the aromatic moiety of each ester. Repetitive scan analyses detected changes in absorbance profile to indicate hydrolytic catalysis by the enzyme. Each compound was found to be hydrolyzed by BuChE but not AChE.

The affinity constant ( $K_m$ ) and maximum velocity ( $V_{max}$ ) for each compound (**1–3**) hydrolyzed by BuChE under the same conditions were obtained from Lineweaver-Burk plots and are summarized in Table 1. The kinetic parameters ( $K_m$  and  $V_{max}$ ) for compounds **1** and **2** are similar to one another but distinctly different from those obtained for the (*R*) *N*-methylpyrrolidinol derivative (**3**). A comparison of the most stable conformations of the three esters (Fig. 3) indicated, as with the kinetic parameters, that the overall preferred conformations of **1** and **2** are similar to one another but distinct from the conformation of compound **3**. These differences in molecular geometries may be largely responsible for the differences in affinities and rates of hydrolysis of compounds **1** and **2** compared to **3**.

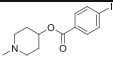
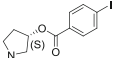
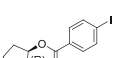
### Synthesis of Tributyltin Intermediates

In order to incorporate  $^{123}\text{I}$  into iodobenzoate esters, a stable intermediate had to be developed with a functionality readily replaced by  $^{123}\text{I}$ . Thus, compounds **1–3** were converted to their corresponding tributyltin intermediates (Fig. 2b) in high (73–78%) yields. These tributyltin intermediates were found to be stable over several months when stored without solvent, in the dark, at 4°C. However, the ester linkage underwent transesterification in methanol and hydrolysis in water, over several days, when diluted in either solvent. Therefore, fresh solutions of tributyltin intermediates were prepared for each radiolabel incorporation reaction described below.

### Radiosynthesis and Purification of $^{123}\text{I}$ -Labeled Iodobenzoates

Incorporation of  $^{123}\text{I}$  into the benzoate esters was achieved in a rapid, one step reaction (Fig. 2c), under mild conditions (15 min, ambient temperature).  $\text{Na}^{123}\text{I}$  was obtained commercially in 0.1 N NaOH, in the minimal volume available. The presence of NaOH in the reaction mixture rapidly hydrolyzed the ester of the tributyltin intermediate and led to lower yields. To circumvent this, the NaOH was first neutralized with a slight excess of 0.1 M HCl. Slightly acidic conditions allowed the reaction to proceed rapidly without ester hydrolysis. *N*-chlorosuccinimide (NCS) was

**Table 1.** Enzyme kinetic and log P values for synthesized iodobenzoate esters 1–3

Compound	Structure	BuChE $K_m$ ( $\mu\text{M}$ )	$V_{\max}$ ( $\mu\text{M min}^{-1}$ )	Log P
1		$26 \pm 2$	$8.4 \pm 0.4$	3.16
2		$16 \pm 4$	$6.1 \pm 0.5$	3.05
3		$50 \pm 2$	$33.2 \pm 2.7$	3.05

used to form *N*- $^{123}\text{I}$ -iodosuccinimide *in situ*. Since the amount of  $^{123}\text{I}$  is limiting in the reaction, non-radioactive NaI was added to the radioactive  $\text{Na}^{123}\text{I}$  population in order to generate a greater amount of product. Purification of the radiolabeled ligand from the reaction mixture was achieved using HPLC with a reverse phase column and 80% methanol<sub>(aq)</sub> as eluent (Fig. 4). Fractions were collected and those containing radiolabeled compound, as predetermined by elution profiles using non-radioactive esters (Fig. 4), were combined and the solvent removed, using a stream of nitrogen gas and gentle heating. The product was redissolved into 20% ethanol<sub>(aq)</sub>. Synthesis and purification of radiolabeled compounds was performed within 1 h, with 63–92% radiochemical yield and 90–96% purity.

### Biodistribution Studies

The dynamic biodistribution of radiolabeled ligands in the rat were monitored over 1 h (Fig. 5). Biodistribution was similar for the three agents. Regions of interest were head (ROI<sub>1</sub>), heart (ROI<sub>2</sub>), and bladder (ROI<sub>3</sub>). As can be seen in the plot in Fig. 5, there was rapid clearance of radioactivity from the blood pool, as indicated by the heart ROI, via the kidneys, as indicated by the bladder ROI. There was also a rapid increase in the radioactivity in the head region (ROI<sub>1</sub>) that remained relatively constant throughout the duration of scanning. Within ROI<sub>1</sub>, a number of structures, including the brain and salivary glands, may accumulate the radioligands. Since the resolution of scanning did not define regional accumulation of radioactivity within the brain itself, autoradiography was performed to provide details of brain distribution.

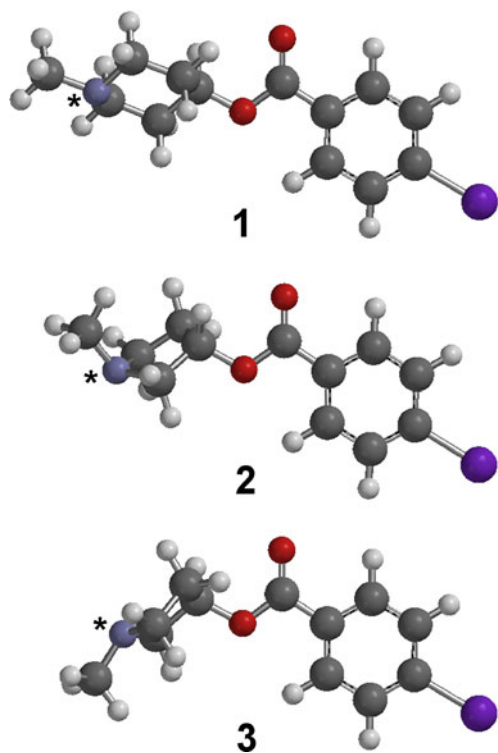


**Fig. 3.** Preferred conformations of compounds 1–3. Note similarity in geometry between compounds 1 and 2 with respect to the position of nitrogen (\*) containing alcohol moiety.

### Comparison of Brain Autoradiography and Butyrylcholinesterase Histochemistry

Autoradiography of brain sections, after injecting any of the radiolabeled iodobenzoates into the normal rat model, revealed that each entered the brain and had a regional distribution, with areas of high and low accumulation, which corresponded to specific neuroanatomical structures (Table 2).

Experimental conditions required to produce brain autoradiograms led to the loss of BuChE enzymatic activity. As a result, the same tissue could not be used for direct comparative BuChE histochemical staining but could be stained with thionin, to visualize cell bodies, for correlation between accumulation of radioactivity and neuroanatomy. These were compared with similar sections from other rat brain tissues, stained for BuChE activity. Figures 6 and 7 provide representative levels for comparison of neuroanatomy, autoradiograms, and BuChE distribution.

Throughout the central nervous system, most areas with low radioactivity corresponded to areas of known low BuChE activity (e.g., cerebral cortex and the caudate putamen; Fig. 6). A number of areas with accumulation of radioactivity corresponded to areas with BuChE activity, as demonstrated by histochemical staining. These areas

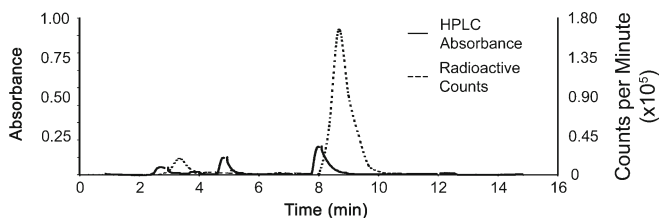


**Fig. 4.** Absorbance traces and radioactive counts demonstrating the separation of radiolabeled compound **1** from the reaction mixture using HPLC. The desired radioactive product has a retention time between 8 and 10 min. The lag in the peaks of the retention times between the absorbance and radioactivity is a consequence of difference in the delivery system to the two different detectors.

included certain thalamic nuclei (e.g., habenula; Fig. 6), pontine nuclei (e.g., laterodorsal, ventral, and pontine tegmentum; Fig. 7), as well as certain nuclei in the medulla oblongata (e.g., hypoglossal and dorsal motor nucleus of the vagus; Fig. 7). However, there were also areas known to have BuChE activity by histochemical observation that did not appear to accumulate radioactivity. These structures included fiber tracts (e.g., the anterior commissure) and the anterior group of the thalamus (Fig. 6). Conversely, a few areas, such as the motor trigeminal nucleus (Fig. 7), without BuChE activity in histochemical analysis, demonstrated uptake of radioactivity.

## Discussion

BuChE activity associated with AD neuropathological structures [12–17], especially in regions of the brain with normally low BuChE activity, makes this enzyme a suitable potential target for molecular neuroimaging in AD. Previous attempts to image this enzyme have met limited success in that the radioimaging results [20, 21, 23] did not correspond to the known histochemical distribution of this enzyme in normal [8–11] or in AD brains [12–17].

Of the three compounds synthesized and examined here, only 1-methylpiperidin-4-yl 4-iodobenzoate (**1**) had been previously synthesized and studied for potential dopamine transporter affinity [26], as an analgesic [31] or an anticonvulsant [32]. However, this compound did not display any of these properties [26, 31, 32]. Its potential as a cholinesterase substrate and/or imaging agent was not previously reported.

The structure of the molecules synthesized and evaluated here provide some advantages as BuChE imaging agents. Based on differences in the known crystal structures of BuChE [33] and AChE [34], the estimated mean volume of the BuChE gorge ( $502 \text{ \AA}^3$ ) is larger than that of AChE ( $302 \text{ \AA}^3$ ) [35] and the BuChE acyl pocket (L286 and V288) is able to accommodate larger acyl moieties, such as the iodobenzoate group. The three iodobenzoate derivatives (compounds **1–3**) possess a bulky aromatic ring providing selectivity towards BuChE over AChE. As a result, all three iodobenzoate esters are selective for BuChE over AChE. Their affinities for BuChE (Table 1) are comparable to the extensively studied substrate for the enzyme, butyrylthiocholine ( $30.9 \text{ \mu M}$ ) [36].

Although the three compounds were specific for BuChE, compounds **1** and **2** had better affinity for this enzyme relative to compound **3**. In order to understand this difference in affinity, and to facilitate future refinement of these lead compounds, computational studies were undertaken. These determinations revealed that the most stable conformations for compounds **1** and **2**, particularly in relation to the *N*-methyl ring system, were similar (Fig. 3). Specifically, the methyl group on the nitrogen of the ring in **1** and **2** point in the same direction, while in **3** this same methyl group points in the opposite direction. Binding of compounds to the active site gorge of BuChE is facilitated by interaction of the nitrogen with W82 of the enzyme active site gorge [33]. These studies indicate that compounds with conformations similar to **1** and **2**, with respect to the nitrogen, would be desirable to improve binding to BuChE for imaging since they have higher affinity and are hydrolyzed more slowly than compound **3**. This would imply a longer time period for the radiolabel to be part of the acylated BuChE complex.

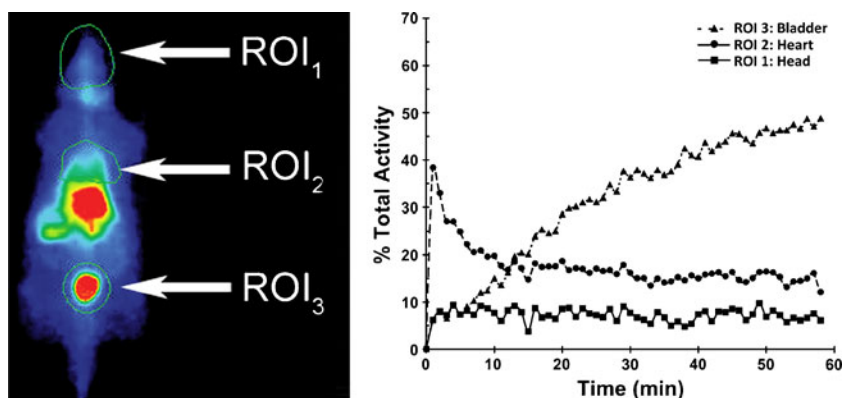


**Fig. 5.** An example of the biodistribution of compound **1** in the rat. Composite images from 60 min of scanning indicate that compounds **1–3** accumulate (*image on the left*) in the head (ROI<sub>1</sub>), heart (ROI<sub>2</sub>), and bladder (ROI<sub>3</sub>). Activity levels (*plots on the right*) were measured in these regions for the duration of imaging.



**Table 2.** Distribution of BuChE and radioactivity accumulation in the rat brain

Area	BuChE activity	Radioactivity
Caudate putamen	–	–
Cerebral cortex	+	+
Hippocampus	+	++
Hypothalamus	+	++
Islands of Calleja	++++	–
Septal region	++	++
Thalamus		
Anterior nuclear group	++++	–
Anterior pretectal nucleus	+++	++
Geniculate nuclear group	+	–
Habenula	++	++
Lateral nuclear group	+++	–
Medial, midline, ventral and posterior nuclear groups	++	–
Zona incerta	++	++
Midbrain		
Inferior colliculus	+	+
Interpeduncular nucleus	+++	–
Oculomotor nucleus	–	++++
Periaqueductal gray	++	++
Red nucleus	++	++++
Superior colliculus	++	++
Pons		
Facial nucleus	++	++++
Lateral dorsal tegmental nucleus	+++	++
Locus coeruleus	++	++
Motor trigeminal nucleus	–	++++
Pedunculopontine tegmental nucleus	+++	++
Pontine nuclei	+	+
Ventral tegmental nucleus	+++	++
Medulla oblongata		
Dorsal motor nucleus of the vagus	++++	++++
Hypoglossal nucleus	++++	++++
Medullary tegmentum	+	++
Spinal trigeminal nuclei	+	+
Vestibular nuclei	++	+++
Cerebellum		
Cerebellar cortex	++	+
Cerebellar nuclei	+	++
White matter		
Anterior commissure	++	–
Corpus callosum	++	–
External capsule	+	–
Fimbria	+	–
Internal capsule	+	–
Pyramidal tract	+	–

For radiosynthesis, the replacement of non-radioactive iodine with  $^{123}\text{I}$  for imaging was found to occur efficiently through a stable tributyltin intermediate (Fig. 2c). This most likely occurred through a free radical mechanism that permitted rapid synthesis. In addition, efficient purification permitted subsequent timely administration into experimental animals. For the present study, to allow recovery of the radiolabeled product in sufficient quantity, albeit at the expense of the desired higher specific radioactivity, non-radioactive iodide was added to favor higher product yield. Incorporation of  $^{123}\text{I}$  in compounds 1–3 occurred in 15 min at ambient temperature and was rapidly purified using HPLC (see Fig. 4 for compound 1 as an example). Total time required for synthesis, purification, and preparation for injection was approximately 1 h, an acceptable time when labeling with  $^{123}\text{I}$ .

The  $^{123}\text{I}$ -labeled compounds showed initial high uptake in the heart ROI, undoubtedly reflecting the initial blood pool (Fig. 5). The blood pool activity diminished rapidly with time. Such quick disappearance was expected since these esters are susceptible to hydrolysis by BuChE in the blood. This was accompanied by a rapid increase in the bladder (ROI<sub>3</sub>), indicating the kidneys were the primary route of excretion (Fig. 5). There was some activity in the neck centrally (Fig. 5) which could include the thyroid gland. This will require further investigations as these compounds are developed further.

Importantly, for the present study, a smaller but significant amount of uptake was also detected in the head region (Fig. 5). *In vivo* scanning resolution was insufficient to definitively establish the distribution within the head to determine whether it included the brain. The rapid clearance

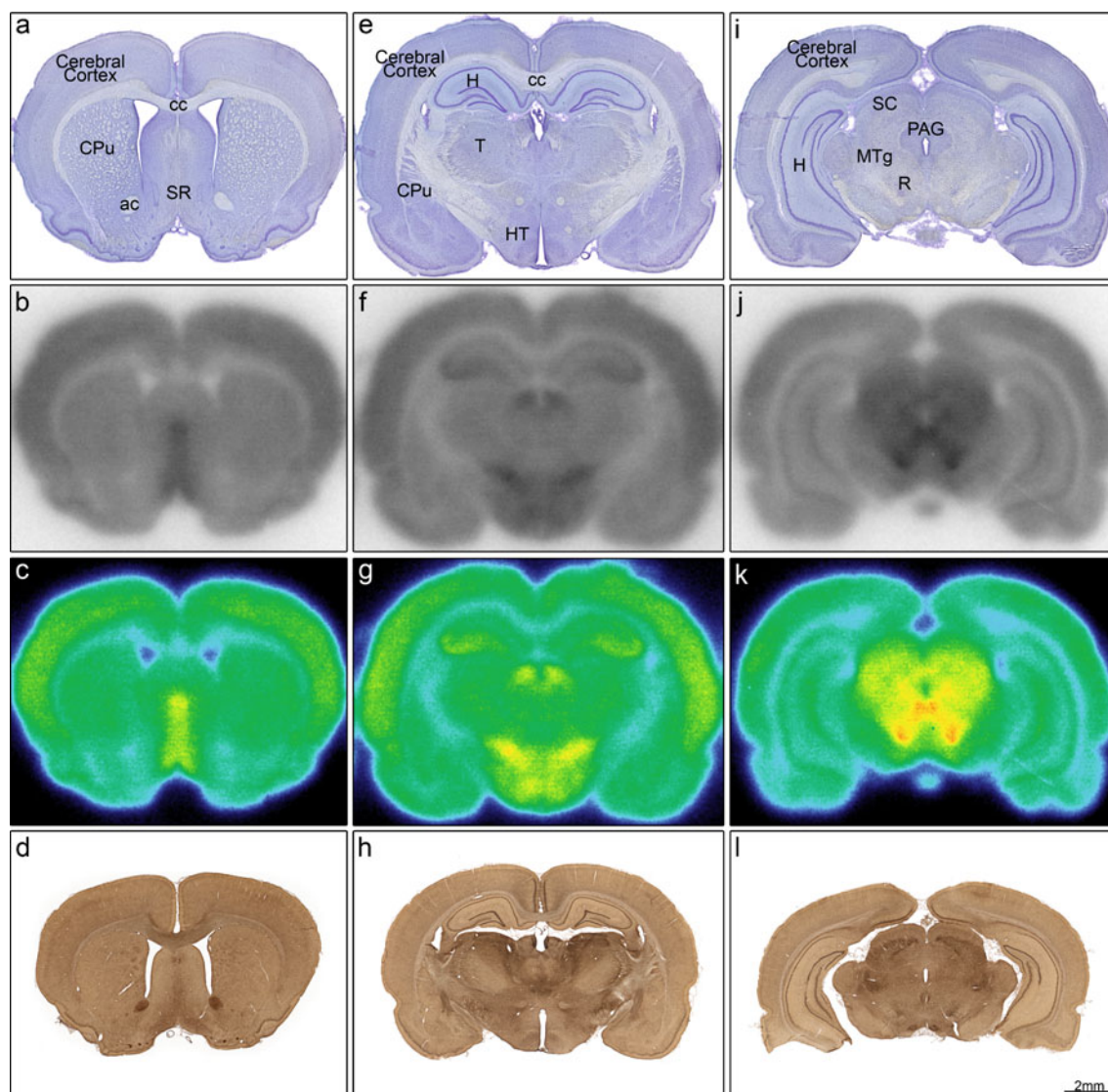


**Fig. 6.** Comparison of neuroanatomy (**a, e, i**), radioactivity distribution (**b, f, j**), and corresponding gradient maps (**c, g, k**), as well as butyrylcholinesterase histochemistry (**d, h, l**) in the rostral aspect of the rat brain. *ac* anterior commissure, *cc* corpus callosum, *CPu* caudate putamen, *H* hippocampus, *HT* hypothalamus, *MTg* midbrain tegmentum, *PAG* periaqueductal gray, *R* red nucleus, *SC* superior colliculus, *SR* septal region, *T* thalamus.

from the blood pool indicated the relatively constant uptake in the head was not simply related to blood perfusion. A metabolic trapping principle [37] of compounds metabolized by enzymes within the brain supported the accumulation observed. Also, it is possible that the limited uptake in the head region, and specifically in the brain, was due to metabolism of the radioligand in the blood.

To determine whether the  $^{123}\text{I}$ -labeled iodobenzoate esters actually accumulated in the brain, and in regions of known BuChE activity, detailed autoradiography of brain sections was carried out and compared to BuChE and thionin staining. Data in Table 2 and in Figs. 6 and 7, confirm a high degree of overlap between radiolabel accumulation and BuChE activity. Importantly, in a region of normally low BuChE activity, such as the cerebral cortex, little uptake of radioactivity was seen (Fig. 6). However,

certain discrepancies were also observed. For example, the motor trigeminal nucleus, that has low BuChE activity in histochemical analyses, displayed high radioactivity accumulation (Fig. 7). This discrepancy may be due to a number of factors, that could include binding of these iodobenzoate esters to other enzymes and receptors unique to such regions. Conversely, in some areas, such as the anterior commissure and the corpus callosum, that exhibit high histochemical BuChE activity (Table 2), little  $^{123}\text{I}$  accumulation was observed in the autoradiograms (Fig. 6). However, in white matter regions, where BuChE activity is high in histochemical analysis, low accumulation of radioactivity may be due to relatively less blood flow to these structures [38]. These issues will require further investigations. Nonetheless, observations presented herein, hold promise that these  $^{123}\text{I}$  iodobenzoate esters, or other more refined but

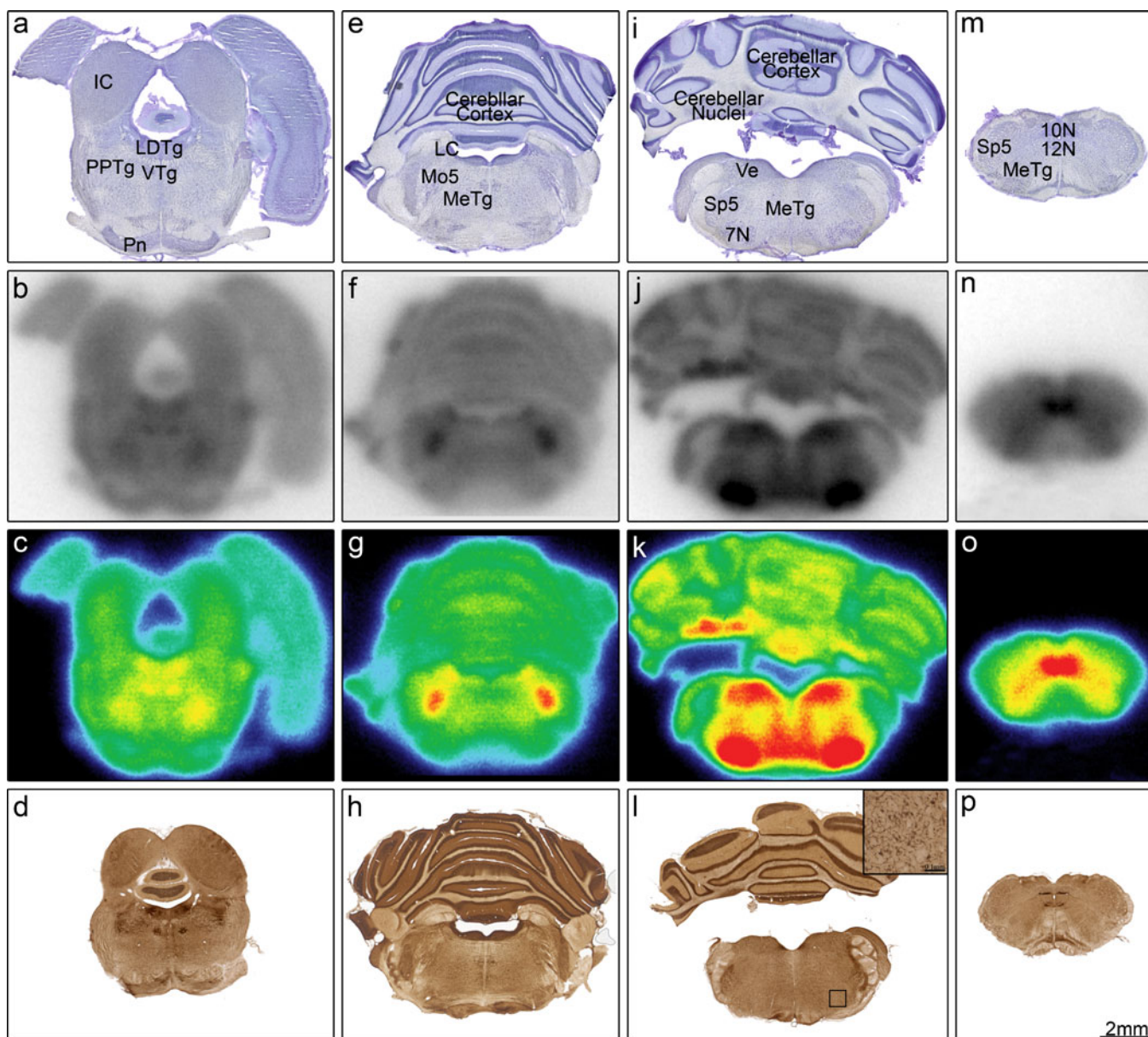


**Fig. 7.** Comparison of neuroanatomy (**a, e, i, m**), radioactivity distribution (**b, f, j, n**), and corresponding gradient maps (**c, g, k, o**), as well as butyrylcholinesterase histochemistry (**d, h, l, p**) in the caudal aspect of the rat brain. *7N* facial nucleus, *10N* dorsal motor nucleus of the vagus, *12N* hypoglossal, *IC* inferior colliculus, *LC* locus coeruleus, *LDTg* lateral dorsal tegmental nucleus, *MeTg* medullary tegmentum, *Mo5* motor trigeminal nucleus, *Pn* pontine nuclei, *PPTg* pedunclopontine tegmental nucleus, *Sp5* spinal trigeminal nucleus, *VTg* ventral tegmental nucleus, *Ve* vestibular nuclei.

comparable derivatives, will be able to detect elevated BuChE activity in the cortex, where this enzyme is associated with the neuropathological structures of AD.

## Conclusion

A total of three potential imaging agents have been synthesized and enzyme kinetic studies have indicated that these compounds have high BuChE affinity and are specific for that enzyme over AChE. Synthetic tributyltin derivatives provided suitable intermediates for incorporation of  $^{123}\text{I}$ . Biodistribution in the rat revealed that the injected radiolabeled compounds are

retained in the head region and autoradiography provided a localized distribution of radioactivity in the brain. Despite some differences between the autoradiograms and histochemical visualization, many areas that are known to contain BuChE corresponded to areas of radioactivity accumulation. Importantly, the region of the brain where BuChE accumulates in association with AD neuropathology, the cerebral cortex, did not exhibit accumulation of iodobenzoate radiolabel in the normal rat brain examined here. Therefore, these reported  $^{123}\text{I}$  iodobenzoate esters show promise in guiding the development of BuChE imaging agents that can detect AD pathology *in vivo*, thus permitting early diagnosis of this disease.

**Acknowledgments.** The Canadian Institutes of Health Research (MOP-82798), Canadian Institutes of Health Research Vascular Health and Dementia Initiative (DOV-78344) (through partnership of Canadian Institutes of Health Research, Heart & Stroke Foundation of Canada, the Alzheimer Society of Canada and Pfizer Canada Inc.), Capital District Health Authority Research Fund, Nova Scotia Health Research Foundation, National Sciences and Engineering Research Council, Canadian Foundation for Innovation, Dalhousie Radiology Research Foundation, Dalhousie University, and Mount Saint Vincent University are gratefully acknowledged. We thank Amy Morris, Marlene Hudgins, Melissa Morash, Anita Macdonald, Simone LaForest, and Eva Rogerson for their technical assistance.

**Conflict of Interest Disclosure.** Application for patent protection has been filed relating to the iodobenzoate esters described in this manuscript, through Treventis Corporation, in which one of the authors (SD) is a shareholder. SD made an invited presentation (possible mechanisms underlying effects of BuChE—emerging hypotheses to spark future research) at a mini-symposium entitled “Emerging hypotheses in cholinesterase inhibition: targeted activity for optimal effects”, organized by Novartis in Geneva as part of the 11th International Geneva/Springfield Symposium on Advances in Alzheimer Therapy. No funding has been received from either of these companies in support of the work described herein.

## References

- Blennow K, de Leon MJ, Zetterberg H (2006) Alzheimer's disease. *Lancet* 368:387–403
- Hyman BT, Trojanowski JQ (1997) Consensus recommendations for the postmortem diagnosis of Alzheimer disease from the national institute on aging and the reagan institute working group on diagnostic criteria for the neuropathological assessment of Alzheimer disease. *J Neuropathol Exp Neurol* 56:1095–1097
- Davies P, Maloney AJ (1976) Selective loss of central cholinergic neurons in Alzheimer's disease. *Lancet* 2:1403
- Bartus RT, Dean RL 3rd, Beer B, Lippa AS (1982) The cholinergic hypothesis of geriatric memory dysfunction. *Science* 217:408–414
- Coyle JT, Price DL, DeLong MR (1983) Alzheimer's disease: a disorder of cortical cholinergic innervation. *Science* 219:1184–1190
- Perry EK, Perry RH, Blessed G, Tomlinson BE (1978) Changes in brain cholinesterases in senile dementia of Alzheimer type. *Neuropathol Appl Neurobiol* 4:273–277
- Mesulam M-M, Geula C (1991) Acetylcholinesterase-rich neurons of the human cerebral cortex: cytoarchitectonic and ontogenetic patterns of distribution. *J Comp Neurol* 306:193–220
- Friede RL (1967) A comparative histochemical mapping of the distribution of butyryl cholinesterase in the brains of four species of mammals, including man. *Acta Anat* 66:161–177 (Basel)
- Darvesh S, Grantham DL, Hopkins DA (1998) Distribution of butyrylcholinesterase in the human amygdala and hippocampal formation. *J Comp Neurol* 393:374–390
- Darvesh S, Hopkins DA (2003) Differential distribution of butyrylcholinesterase and acetylcholinesterase in the human thalamus. *J Comp Neurol* 463:25–43
- Darvesh S, Hopkins DA, Geula C (2003) Neurobiology of butyrylcholinesterase. *Nat Rev Neurosci* 4:131–138
- Friede RL (1965) Enzyme histochemical studies of senile plaques. *J Neuropathol Exp Neurol* 24:477–491
- Geula C, Mesulam M-M (1989) Special properties of cholinesterases in the cerebral cortex of Alzheimer's disease. *Brain Res* 498:185–189
- Mesulam M-M, Geula C (1994) Butyrylcholinesterase reactivity differentiates the amyloid plaques of aging from those of dementia. *Ann Neurol* 36:722–727
- Geula C, Mesulam M-M (1995) Cholinesterases and the pathology of Alzheimer disease. *Alzheimer Dis Assoc Disord* 9(Suppl 2):23–28
- Guillozet AL, Smiley JF, Mash DC, Mesulam M-M (1997) Butyrylcholinesterase in the life cycle of amyloid plaques. *Ann Neurol* 42:909–918
- Darvesh S, Reid GA, Martin E (2010) Biochemical and histochemical comparison of cholinesterases in normal and Alzheimer brain tissues. *Curr Alzheimer Res* 7:386–400
- Snyder SE, Gunupudi N, Sherman PS et al (2001) Radiolabeled cholinesterase substrates: *in vitro* methods for determining structure-activity relationships and identification of a positron emission tomography radiopharmaceutical for *in vivo* measurement of butyrylcholinesterase activity. *J Cereb Blood Flow Metab* 21:132–143
- Kikuchi T, Fukushi K, Ikota N, Ueda T, Nagatsuka S, Arano Y, Irie T (2001) Synthesis of piperidinyl and pyrrolidinyl butyrates for potential *In Vivo* measurement of cerebral butyrylcholinesterase activity. *J Labelled Cpd Radiopharm* 44:31–41
- Kikuchi T, Zhang MR, Ikota N, Fukushi K, Okamura T, Suzuki K, Arano Y, Irie T (2004) N-[18 F]fluoroethylpiperidin-4-ylmethyl butyrate: a novel radiotracer for quantifying brain butyrylcholinesterase activity by positron emission tomography. *Bioorg Med Chem Lett* 14:1927–1930
- Roivainen A, Rinne J, Virta J, Järvenpää T, Salomäki S, Yu M, Nägren K (2004) Biodistribution and blood metabolism of 1–11 C-methyl-4-piperidinyl n-butyrate in humans: an imaging agent for *in vivo* assessment of butyrylcholinesterase activity with PET. *J Nucl Med* 45:2032–2039
- Virta JR, Tolvanen T, Nagren K, Bruck A, Roivainen A, Rinne JO (2008) 1–11 C-methyl-4-piperidinyl-N-butyrate radiation dosimetry in humans by dynamic organ-specific evaluation. *J Nucl Med* 49:347–353
- Kuhl DE, Koeppe RA, Snyder SE, Minoshima S, Frey KA, Kilbourn MR (2006) *In vivo* butyrylcholinesterase activity is not increased in Alzheimer's disease synapses. *Ann Neurol* 59:13–20
- Tago H, Maeda T, McGeer PL, Kimura H (1992) Butyrylcholinesterase-rich neurons in rat brain demonstrated by a sensitive histochemical method. *J Comp Neurol* 325:301–312
- Darvesh S, Smereczynsky A, Hopkins DA (1992) Distribution of butyrylcholinesterase in the rat brain. *Neurosci Abstr* 18:1505 (Abstract)
- Singh S, Basmadjian GP, Avor KS, Pouw B, Seale TW (1997) Synthesis and ligand binding studies of 4'-iodobenzoyl esters of tropanes and piperidines at the dopamine transporter. *J Med Chem* 40:2474–2481
- Darvesh S, Kumar R, Roberts S, Walsh R, Martin E (2001) Butyrylcholinesterase-mediated enhancement of the enzymatic activity of trypsin. *Cell Mol Neurobiol* 21:285–296
- Irvine CA (2006) Spartan '06 Wave function Inc
- Tetko IV, Tanchuk VY, Villa AE (2001) Prediction of n-octanol/water partition coefficients from PHYSPROP database using artificial neural networks and E-state indices. *J Chem Inf Comput Sci* 41:1407–1421
- Darvesh S, Walsh R, Kumar R, Caines A, Roberts S, Magee D, Rockwood K, Martin E (2003) Inhibition of human cholinesterases by drugs used to treat Alzheimer disease. *Alzheimer Dis Assoc Disord* 17:117–126
- Cheng CY, Brochmann-Hanssen E, Waters JA (1982) Quantitative structure-activity relationships of aromatic esters of 1-methyl-4-piperidinol as analgesics. *J Med Chem* 25:145–152
- Waters JA, Hollingsworth EB, Daly JW, Lewandowski G, Creveling CR (1986) Anticonvulsant activity of piperidinol and (dialkylamino) alkanol esters. *J Med Chem* 29:1512–1516
- Nicolet Y, Lockridge O, Masson P, Fontecilla-Camps JC, Nachon F (2003) Crystal structure of human butyrylcholinesterase and of its complexes with substrate and products. *J Biol Chem* 278:41141–41147
- Sussman JL, Harel M, Silman I (1993) Three-dimensional structure of acetylcholinesterase and of its complexes with anticholinesterase drugs. *Chem Biol Interact* 87:187–197
- Saxena A, Redman AM, Jiang X, Lockridge O, Doctor BP (1997) Differences in active site gorge dimensions of cholinesterases revealed by binding of inhibitors to human butyrylcholinesterase. *Biochemistry* 36:14642–14651
- Kikuchi T, Okamura T, Fukushi K, Takahashi K, Toyohara J, Okada M, Zhang MR, Irie T (2007) Cerebral acetylcholinesterase imaging: development of the radioprobes. *Curr Top Med Chem* 7:1790–1799
- Vaucher E, Borredon J, Seylaz J, Lacombe P (1995) Autoradiographic distribution of cerebral blood flow increases elicited by stimulation of the nucleus basalis magnocellularis in the unanesthetized rat. *Brain Res* 691:57–68